International Journal of Nanomedicine

Dovepress
Taylor & Francis Group

Open Access Full Text Article

ORIGINAL RESEARCH

Evaluation of Anti-Inflammatory and Antibacterial Properties of Photo-Thermal Hydrogel as Dual Functional Platform for Management of Periodontitis

Zhisong Mai[1], Yuying Mai[1], Xianxian Huang[1], Shipeng Ning[2], Hongbing Liao[3]

[1]Department of Prosthodontics, College of Stomatology, Guangxi Medical University, Nanning, Guangxi, 530021, People's Republic of China; [2]Research Center of Nanomedicine Technology, the Second Affiliated Hospital of Guangxi Medical University, Nanning, 530000, People's Republic of China; [3]Guangxi Key Laboratory of Oral and Maxillofacial Rehabilitation and Reconstruction, College of Stomatology, Guangxi Medical University, Nanning, Guangxi, 530021, People's Republic of China

Correspondence: Hongbing Liao, Email hongbing_liao@gxmu.edu.cn

Background: Periodontitis, one of the most common oral diseases caused by bacterial infection which affects gums, periodontal ligament and alveolar bone, is a leading cause of tooth loss in adults. Current clinical treatments, such as scaling or antibiotics, often result in incomplete biofilm removal or can contribute to drug resistance.

Methods: To address these limitations, a nanozyme comprising platinum, copper, and selenium was developed, which was then incorporated into a thermoresponsive hydrogel.

Results: When applied to periodontal pockets and exposed to 808 nm laser irradiation, the hydrogel became soft, dissolving to release the nanozyme. This nanozyme demonstrated superoxide dismutase (SOD)-like and catalase (CAT)-like activity, reducing excess reactive oxygen species (ROS) while displaying strong antibacterial and anti-inflammatory effects.

Conclusion: This photothermal nanozyme hydrogel showed excellent biocompatibility and has the potential to overcome the challenges of current periodontitis treatments.

Keywords: thermosensitive, photothermal therapy, hydrogel, periodontitis

Introduction

Periodontitis, a common oral disease encountered in clinical practice, is a chronic inflammation affecting the gingiva and periodontal tissues, primarily caused by dental plaque and calculus.[1–3] Its prevalence increases with age, affecting a significant portion of middle-aged individuals. Periodontitis is not only a major contributor to tooth loss but is also considered a risk factor for cardiovascular diseases, ultimately impacting patients' quality of life.[4,5]

The oral environment is moist, warm, and nutrient-rich, allowing external bacteria to proliferate, adhere to teeth, and migrate along their surfaces.[6,7] This leads to the formation of periodontal pockets and subsequent tissue inflammation. Treatment approaches for periodontitis include both non-surgical and surgical options.[8] For mild to moderate cases, scaling and occasionally antibiotics are used; however, advanced periodontitis often requires the removal of subgingival infections and bacteria from periodontal pockets, sometimes necessitating surgical interventions such as soft tissue and bone grafting to prevent tooth loss.[9–11] These treatments are often painful, and antibiotic use may result in incomplete biofilm removal in deep pockets, promoting bacterial resistance and reducing treatment efficacy.[12,13] Furthermore, uncontrolled drug release can limit therapeutic effectiveness. Given the role of excessive reactive oxygen species (ROS) in driving inflammation in periodontitis, it is essential to develop innovative therapies with controlled, extended drug release that provide both antibacterial and anti-inflammatory effects.

Received: 17 December 2024
Accepted: 27 February 2025
Published: 11 March 2025

Recent studies have highlighted innovative nanomedicine approaches for disease treatment including periodontitis.[14–19] Effective therapy for periodontitis hinges on reducing inflammation and promotion tissue recovery.[20] To this end, numerous advanced nanoplatforms have been developed to enhance the periodontal microenvironment.[21–23] Certain nanoparticles with inherent antibacterial properties can effectively disrupt plaque biofilms.[16,24,25] Unlike standard antibiotic therapy, these nanoplatforms minimize the possibility of antimicrobial resistance. For instance, a nanoplatform based on AuAg nanoparticles was shown to reduce bacterial presence and lower ROS levels under near-infrared (NIR) laser irradiation, thereby facilitating tissue healing in surrounding areas.[26] Other approaches focus on modulating the microenvironment, such as through ROS scavenging, to support tissue repair.[27–29] Chen's team reported that nanoparticles derived from green tea effectively clear excessive ROS to treat periodontitis, also could modulate the inflammatory microenvironment.[30] Other nanomaterial designs, such as cerium oxide nanoparticles, utilize enzyme-mimicking characteristics, known as nanozyme activity, to eliminate hydroxyl radicals through superoxide dismutase (SOD)-like properties.[31] For instance, Wang's team reported a self-assembled nanozyme platform for treatment of periodontitis by its SOD and catalase (CAT) activity.[32] Wei's team developed a glutathione peroxidase (GPx) mimicking nanozyme which consumed ROS and remodeled bone.[33] However, achieving controlled, sustained release of nanodrugs to maintain therapeutic efficacy throughout treatment remains a significant challenge.

Photothermal therapy (PTT), which converts light energy into heat via specific mediating agents, is gaining traction in disease treatment. Noble metals like bismuth, gold, silver, and platinum absorb light energy, exciting electrons to release heat.[34–36] Organic agents, including carbon nanomaterials, black phosphorus, and MXenes, also demonstrate efficient PTT conversion with enhanced biocompatibility.[37–39] Studies have shown that some PTT agents can effectively eliminate bacteria, making them promising for periodontitis treatment.[40–44] Leveraging these advantages, a nanozyme hydrogel was designed specifically for periodontitis therapy (Scheme 1). First, the PtCuSe nanozyme—composed of platinum (Pt), copper (Cu), and selenium (Se)—was synthesized via chemical reduction. Pt based nanozymes were reported to possess CAT like activity.[45] Both Se and Cu composed nanozymes showed potential in ROS scavenging due to SOD mimic activity.[46,47] We assumed that the nanozyme composed of Pt/Cu/Se might show potential in CAT/SOD catalytic activity. This nanozyme was then combined with a low-temperature hydrogel to form a uniform solution, which was applied to periodontal pockets and tooth surfaces, forming a stable hydrogel layer. Under 808 nm laser irradiation, the nanozyme's PTT conversion raised the mixture's temperature. This thermo responsive hydrogel became soft triggered by NIR irradiation and release the nanozyme cargo. Acting as a ROS scavenger with both SOD-like and CAT-like properties,

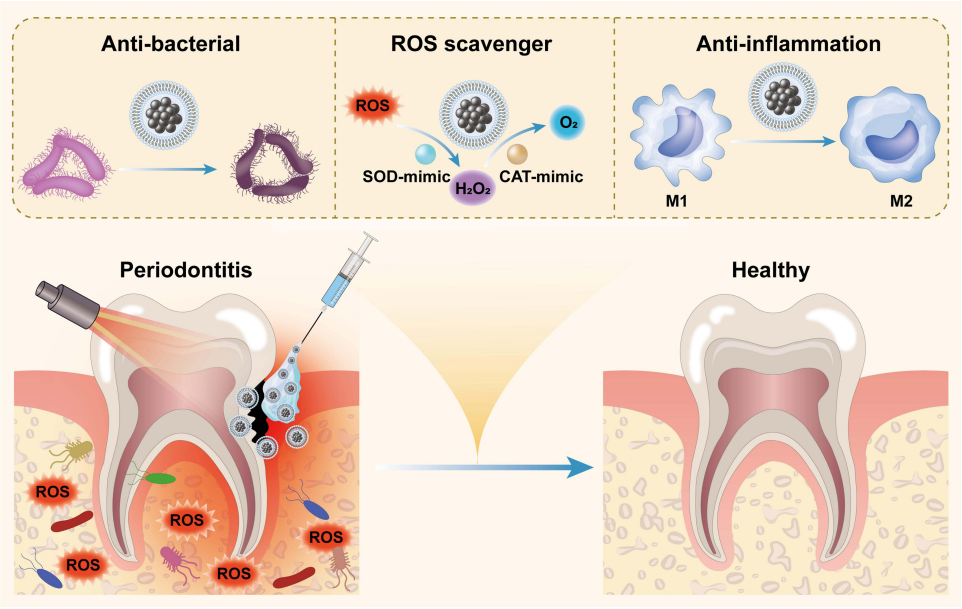

Scheme 1 PtCuSe nanozyme hydrogel for periodontitis treatment by anti-bacterial, ROS-scavenging, and anti-inflammatory action.

this PTT-activated nanozyme hydrogel demonstrated potent antibacterial and disinfecting effects. It also promoted M2 macrophage polarization, supporting anti-inflammatory responses. Both in vitro and in vivo results confirmed that this innovative, biocompatible approach is an effective method for periodontitis treatment.

Materials and Methods

Chemicals

Copper chloride (98%) and Sodium selenite pentahydrate (98%) were purchased from Aladdin (Shanghai). Polyvinylpyrrolidone (PPV), chloroplatinic acid (AR), methanol (AR) were obtained from Sinopharm (Shanghai). All reagents were used without further purify.

Characterization

The morphology of PtCuSe was captured using transmission electron microscope (TEM). Surface analysis of the PtCuSe was carried out using X-ray photoelectron spectroscopy (XPS). Scanning electron microscope (SEM) was applied for observation of PtCuSe hydrogel. An ultraviolet-visible absorption spectrometry (UV-VIS) was used for measurement of absorbance of PtCuSe solution.

Synthesis of PtCuSe Nanozyme

First, 1 mL of methanol solutions of chloroplatinic acid, copper chloride, and sodium selenite (each at a concentration of 7 mg/mL) were added dropwise to 5 mL of polyvinylpyrrolidone (PVP) methanol solution (13.2 mg/mL) under continuous stirring. The reaction mixture was then refluxed and heated for 3 hours. After the reaction, the methanol was removed by rotary evaporation, followed by the addition of 10 mL deionized water. The resulting solution was dialyzed and subsequently lyophilized for further use.

Synthesis of PtCuSe Nanozyme Hydrogel

Next, agarose with low melting property (Yarebio) was dissolved at under stirring at 70 °C (8% w/v) until the solution became clear. During the process, PtCuSe was added with a final concentration of 2 mg/mL to obtain PtCuSe nanozyme hydrogel.

Flow Cytometry Analysis

RAW264.7 cells (Procell, China) were seeded in 6-well plates at a density of 1×10^6 cells/well. After 24 h, cells were treated in different groups including Negative, Control, LPS and LPS+PtCuSe+NIR. Then CD86 expression of RAW 264.7 cells in each group was detected using a flow cytometry analyzer.

Hemolysis Assay

Blood samples were collected from healthy C57BL/6J mice. Next, red blood cells (RBC) were separated by centrifugation for preparation of RBC suspension. Then PtCuSe was added into RBS suspension at different concentrations. Saline and DI water was added as negative and positive control respectively. After 2 h, supernatants were collected after centrifugation (1500 rpm) and absorbance at 540 nm was measured using a Microplate reader.

In Vitro Anti-Planktonic Bacterial Ability Test

For bacterial biofilm formation, experiments were conducted using a concentration of approximately 10^9 CFU/mL. Porphyromonas gingivalis (P. gingivalis) was subjected to various treatments including: (1) Control; (2) NIR; (3) PtCuSe; (4) PtCuSe+NIR. The final concentration of PtCuSe in group (3) and (4) was 100 μg/mL and an 808 nm laser with a density of 1 W/cm^2 was applied for light irradiation for 1 min. 80 μL of each bacterial suspension was spread on blood agar plates, which were incubated anaerobically at 37°C for 5 days. The remaining suspensions were transferred to a 96-well plate for optical density measurement at 600 nm. Similar bacterial biofilms on agar plates in each group were prepared using Staphylococcus aureus (S. aureus) and Escherichia coli (E. coli).

qRT-PCR Measurements

After polarization by LPS, RAW 264.7 cells were divided into 5 groups: (1) Control; (2) LPS; (3) LPS+NIR; (4) LPS +PtCuSe; (5) LPS+PtCuSe+NIR. The final concentration of PtCuSe in group (4) and (5) was 100 μg/mL and an 808 nm laser with a density of 1 W/cm^2 was applied for light irradiation for 1 min. Then the supernatant of culture medium and cells in each group were collected. First the total RNA of RAW 264.7 cells was extracted. After reversion transcribed into cDNA, RNA level was measured using a real-time fluorescence quantitative polymerase chain reaction (qRT-PCR) test system in various treatment groups.

Animal Models

Male C57BL/6J mice aged 8 weeks were purchased from Vital River (Beijing). After the mice were weighed and anesthetized by intraperitoneal injection of 2% tribromoethanol at a dose of 20 mL/kg of body weight, the periodontitis model was established on the right side of the maxilla. First, the interproximal space between the first and second molars was separated and 5–0 silk thread was used for ligatures. A 3 mm bent end of the ligature is placed subgingivally to avoid damaging the oral soft tissue while preserving the integrity of the gingival epithelium. The mice are then placed on a heating pad to recover.

Periodontitis Treatment Efficacy in Vivo

After a week of establishment of models, mice were separated into (1) Sham; (2) PBS; (3) NIR; (4) PtCuSe; (5) PtCuSe +NIR. PtCuSe (2 mg/mL, 10 μL) was injected through gingivals sulcus and 5 min laser irradiation with an 808 nm laser with a density of 1 W/cm^2 was performed. Finally, the maxilla with teeth on the model side is harvested and fixed for hematoxylin and eosin (H&E) staining, Masson staining and microcomputed tomography (microCT) analysis.

Biosafety Evaluation in Vivo

Healthy male C57BL/6J mice were divided into two groups with various treatment including: (1) Control; (2) PtCuSe +NIR. 14 days After treatment, blood samples were harvest for biochemistry test.

Results and Discussion

The PtCuSe nanozyme was first synthesized using a chemical reduction method. Transmission electron microscopy (TEM) images (Figure 1A) show that the PtCuSe nanozyme exhibits an ultrasmall nanoparticle morphology. After being incorporated into an agarose gel, the resulting PtCuSe nanozyme hydrogel is shown in Figure 1B. Elemental mapping proved that Pt, Cu and Se dispersed in hydrogel (Figure 1C). To further analyze the surface chemical composition, X-ray photoelectron spectroscopy (XPS) was conducted, confirming the presence of Pt, Cu and Se within the nanozyme (Figure S1). Further analysis of high-resolution spectra of Pt, Cu and Se verified the chemical property of the nanozyme. As shown in Figure 1D, both Pt (0) and Pt (IV) existed in the nanozyme with atomic percentage of 85% and 15% respectively. Cu orbit analysis in Figure 1E verified the Cu (I)/Cu and Cu (II) in PtCuSe. Finally, it can be inferred that both Se (II) and Se (IV) was included in this nanozyme (Figure 1F). Next, the CAT and SOD-like properties of the nanozyme at different concentrations were evaluated. As illustrated in Figure 1G, PtCuSe incubated with H_2O_2 resulted in significant O_2 release compared to H_2O_2 alone, with higher PtCuSe concentrations yielding greater O_2 production efficiency. PtCuSe demonstrated the ability to scavenge toxic •OH and $•O_2^-$ radicals, as shown in Figure 1H and 1. The scavenging efficiency for both •OH and $•O_2^-$ was concentration-dependent, with PtCuSe at 200 μg/mL removing over 40% of •OH and 60% of $•O_2^-$. These results confirm that the PtCuSe nanozyme was successfully synthesized with robust dual CAT- and SOD-like activities.

The photothermal performance of the PtCuSe nanozyme was subsequently assessed. Using an 808 nm laser at an energy density of 1 W/cm², PtCuSe solutions at various concentrations were irradiated. Results indicated that the PtCuSe nanozyme exhibited concentration-dependent photothermal activity (Figure 2A). At a concentration of 20 μg/mL, the solution's temperature rose above 45°C within 5 min of irradiation, reaching a therapeutically effective level. Further, the nanozyme's photothermal response remained stable over multiple heating and cooling cycles (Figure 2B), demonstrating its photothermal stability. The calculated photothermal conversion efficiency of PtCuSe was 18.4%, significantly higher than that of commercial indocyanine green-5-carboxylic acid (ICG) at 3.1% (Figure 2C and D). The PtCuSe nanozyme also displayed broad-

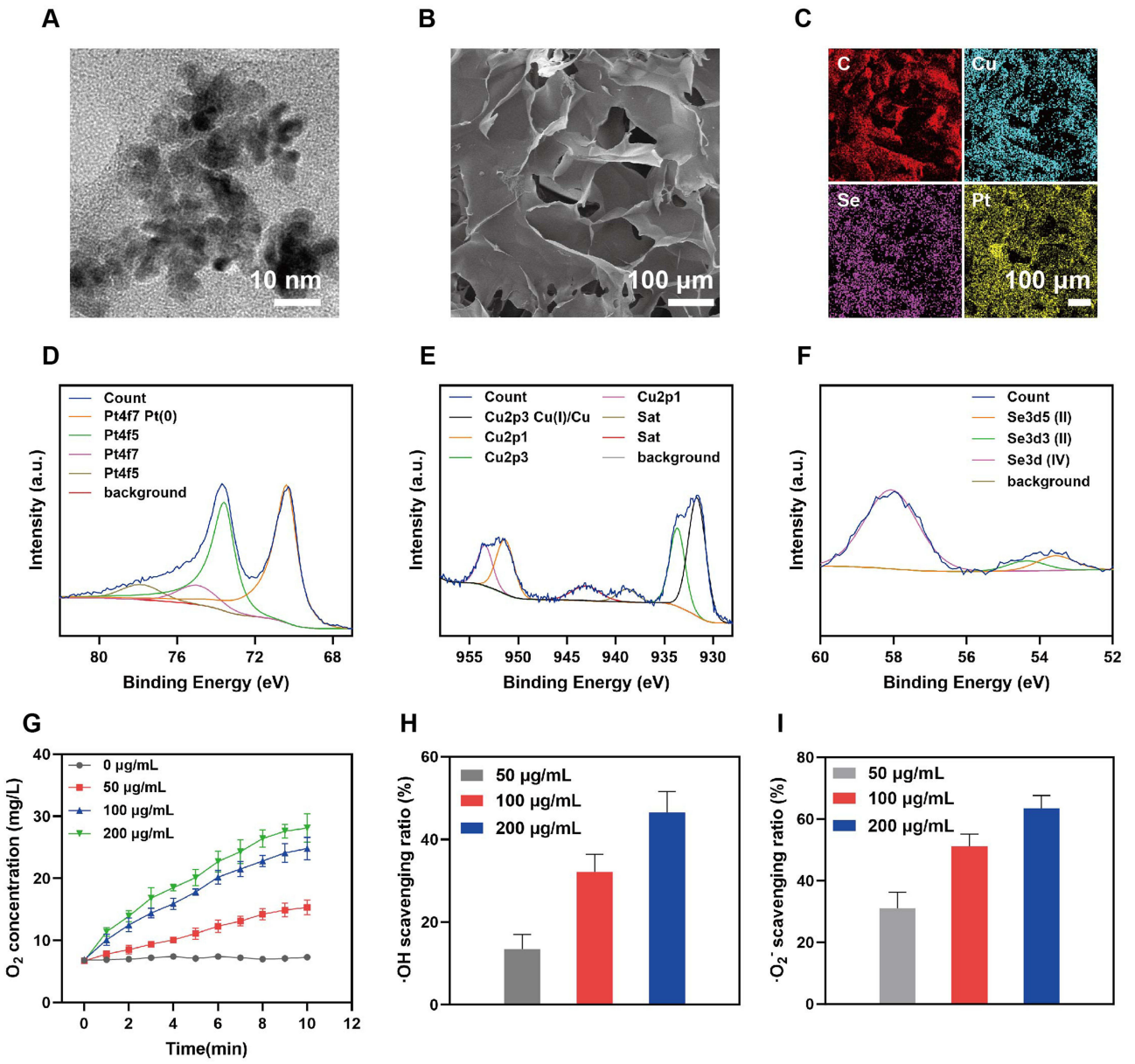

Figure 1 Characterization. (**A**) TEM images of PtCuSe nanozyme. (**B**) SEM images of nanozyme hydrogel. (**C**) Elemental mapping of nanozyme hydrogel. (**D**) Pt high-resolution spectrum. (**E**) Cu high-resolution spectrum. (**F**) Se high-resolution spectrum. (**G**) O_2 generation in H_2O_2 solution with various concentrations of PtCuSe. Scavenging behavior of (**H**) ·OH and (**I**) O_2^-.

wavelength absorption, enhancing its potential as a photothermal agent and thereby PtCuSe nanozyme hydrogel became soft effectively under 808 nm laser irradiation. The appearance of hydrogel remained consistent in at 37 °C after a week which verified its stability in this atmosphere (Figure S2). Overall, PtCuSe was shown to be an excellent candidate for mild photothermal therapy.

Before conducting in vivo applications, the biocompatibility of the PtCuSe nanozyme was evaluated. PtCuSe was introduced into cell culture medium at concentrations ranging from 0 to 200 μg/mL to assess its impact on cell viability in Raw 264.7 cells. As shown in Figure 3A, most of cell survived after co-incubation with PtCuSe at various concentrations. Further analysis using CCK-8 kit in Figure 3B confirmed that cell viability remained above 90% even at the highest concentration of 200 μg/mL, indicating excellent cytocompatibility. Hemolysis rate analysis was conducted to examine hemocompatibility, and as shown in Figure 3C, no significant hemolysis was observed at 200 μg/mL. Overall, these results demonstrate that the PtCuSe nanozyme has an outstanding degree of biocompatibility.

https://doi.org/10.2147/IJN.S508864

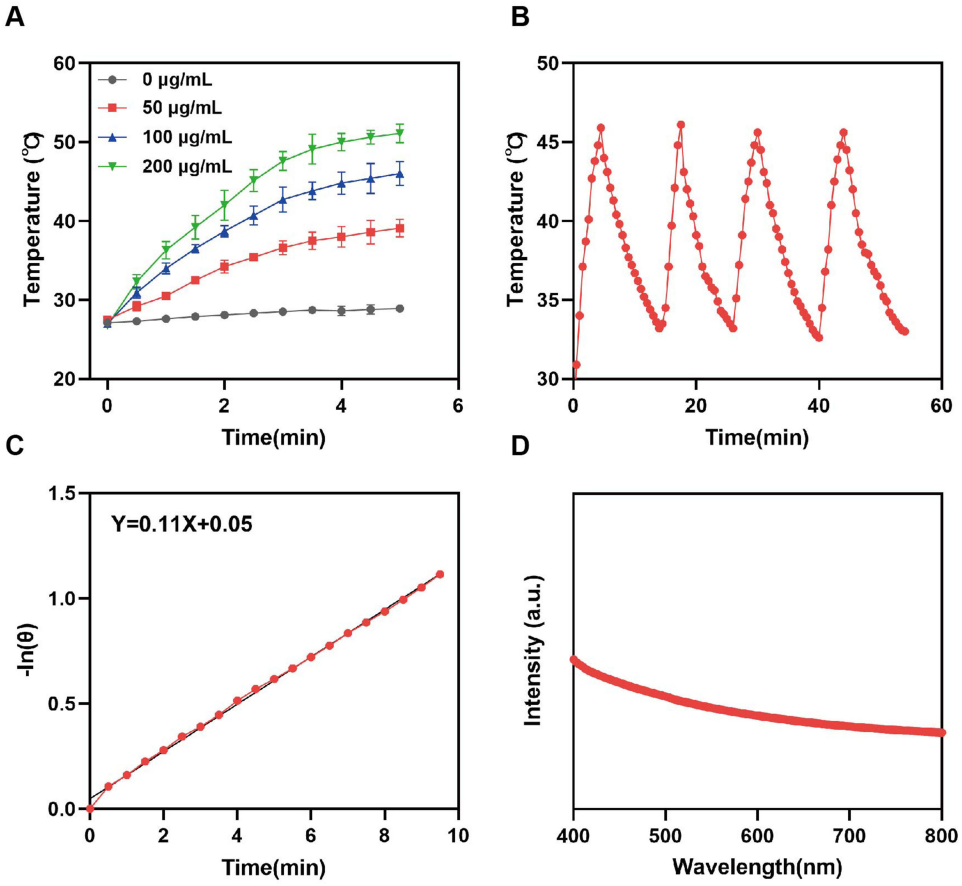

Figure 2 Photothermal performance of PtCuSe nanozyme hydrogel. (**A**) The photothermal effect of PtCuSe nanozyme hydrogel under various treatments. (**B**) Temperature change profiles with repeated irradiation cycles. (**C**) Photothermal conversion efficiency calculation. (**D**) UV-vis absorption spectra.

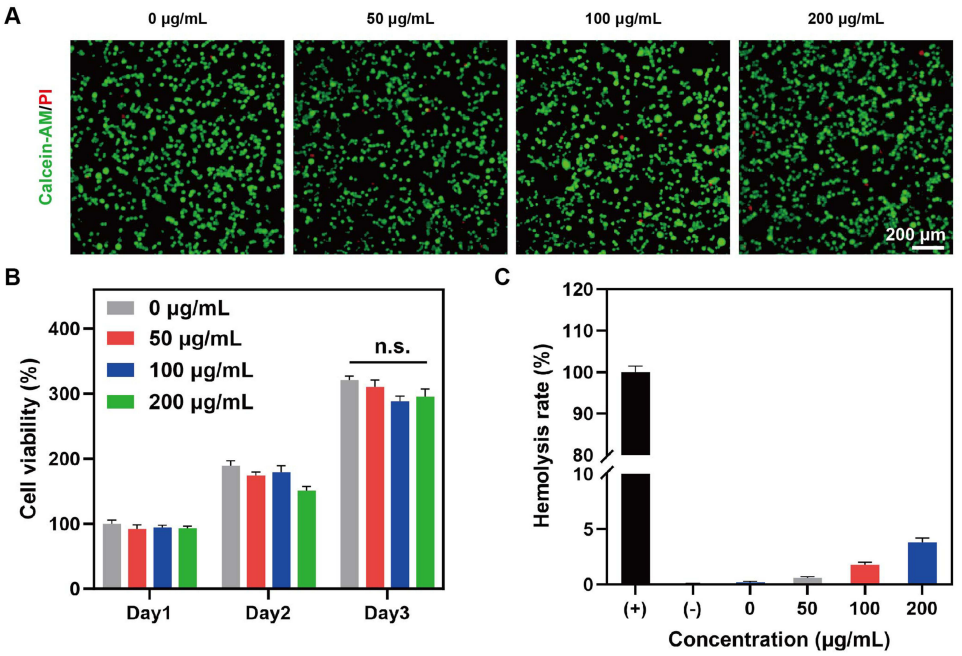

Figure 3 Evaluation of biocompatibility. (**A**) Live/dead fluorescence images of Raw 264.7 cells were co-incubated with PtCuSe at various concentrations (green representing live cells and red representing dead cells). (**B**) Cell cytotoxicity of Raw 264.7 cells co-incubated with PtCuSe hydrogel at various concentrations and time points. (**C**) Hemolysis rate test results. Data are presented as mean ± SD. (n=3).

The antibacterial effect of PtCuSe combined with NIR irradiation was next evaluated using a plate-counting method. *P. gingivalis*, a primary pathogen in periodontitis that damages the immune system and periodontal supporting tissues, was selected alongside *E. coli* and *S. aureus* for antibacterial assessment. Representative plate images of various bacteria under different treatments are shown in Figure 4A. There was no significant difference between the Control and NIR-only groups, suggesting that NIR alone had minimal antibacterial activity. With PtCuSe treatment alone, bacterial counts decreased, though visible colonies remained. In contrast, the PtCuSe + NIR treatment showed marked bacterial inhibition, demonstrating maximum antibacterial efficacy.

Quantitative antibacterial rates for *P. gingivalis, E. coli*, and *S. aureus* are presented in Figure 4B–D. The PtCuSe + NIR treatment achieved the highest elimination rate for *P. gingivalis*, exceeding 80%. Meanwhile, among all treatments, PtCuSe + NIR displayed the most substantial antibacterial effects on both *E. coli* as well as *S. aureus*, while PtCuSe alone provided comparatively lower antibacterial rates. For *P. gingivalis*, the photothermal effect mediated by PtCuSe increased the antibacterial rate by 1.3 times compared to PtCuSe alone. In addition, the antibacterial rate of PtCuSe + NIR group was higher than that in PtCuSe group for both *E. coli* and *S. aureus*. These results demonstrate the potent antibacterial properties of PtCuSe + NIR, highlighting its potential in periodontitis treatment.

The anti-inflammatory effects of PtCuSe combined with NIR were evaluated by investigating macrophage polarization. Initially, inflammation was induced using lipopolysaccharide (LPS). The expression levels of cytokines, including tumor necrosis factor-alpha (TNF-α), an M1-related pro-inflammatory cytokine, and transforming growth factor-beta (TGF-β), an M2-related anti-inflammatory cytokine, were measured using quantitative PCR (qPCR). As shown in Figure 5A and B the LPS group exhibited a significant increase in mRNA expression of TNF-α and a decrease in TGF-β. In stark contrast, the LPS+PtCuSe + NIR group demonstrated significant suppression of the pro-inflammatory cytokine TNF-α while promoting the expression of the anti-inflammatory cytokine TGF-β. The expression of CD86, a marker associated with M1-type macrophages, was analyzed using flow cytometry. Figure 5C illustrates that the number of CD86+ in the PtCuSe + NIR group was significantly reduced compared to the LPS group, which is supported by the representative flow cytometry images shown in Figure 5D–G. Since excessive ROS plays an important role in oxidative damage, we examined the ROS content in cells after various treatments. As shown in Figure 5H, ignorable green fluorescence signal was detected in both Negative and control group while by contrast,

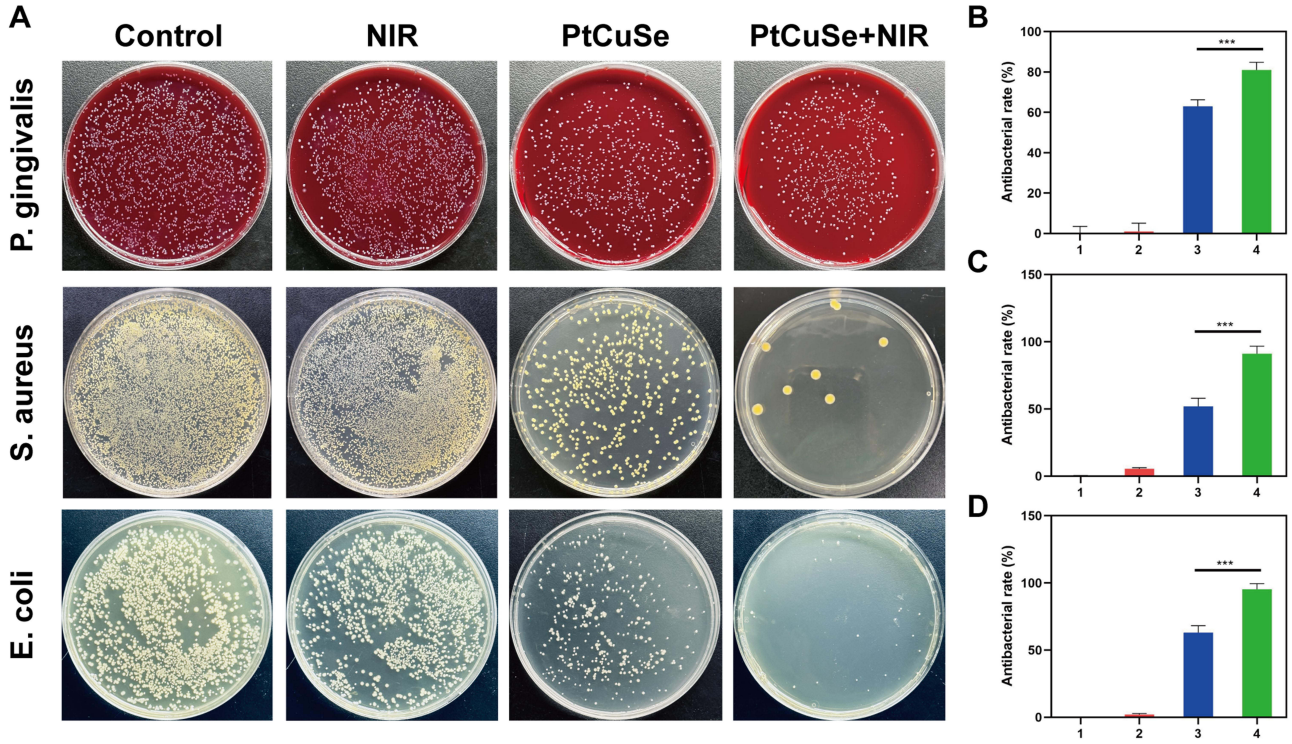

Figure 4 Evaluation of antibacterial potential. (**A**) Representative photographs showing bacterial viability. Antibacterial rate of various treatment groups against (**B**) *P. gingivalis*, (**C**) *S. aureus*, and (**D**) *E. coli*. group 1: control; group 2: NIR; group 3: PtCuSe; group 4: PtCuSe+NIR. Data are presented as mean ± SD. (n=3), *** p<0.001.

https://doi.org/10.2147/IJN.S508864

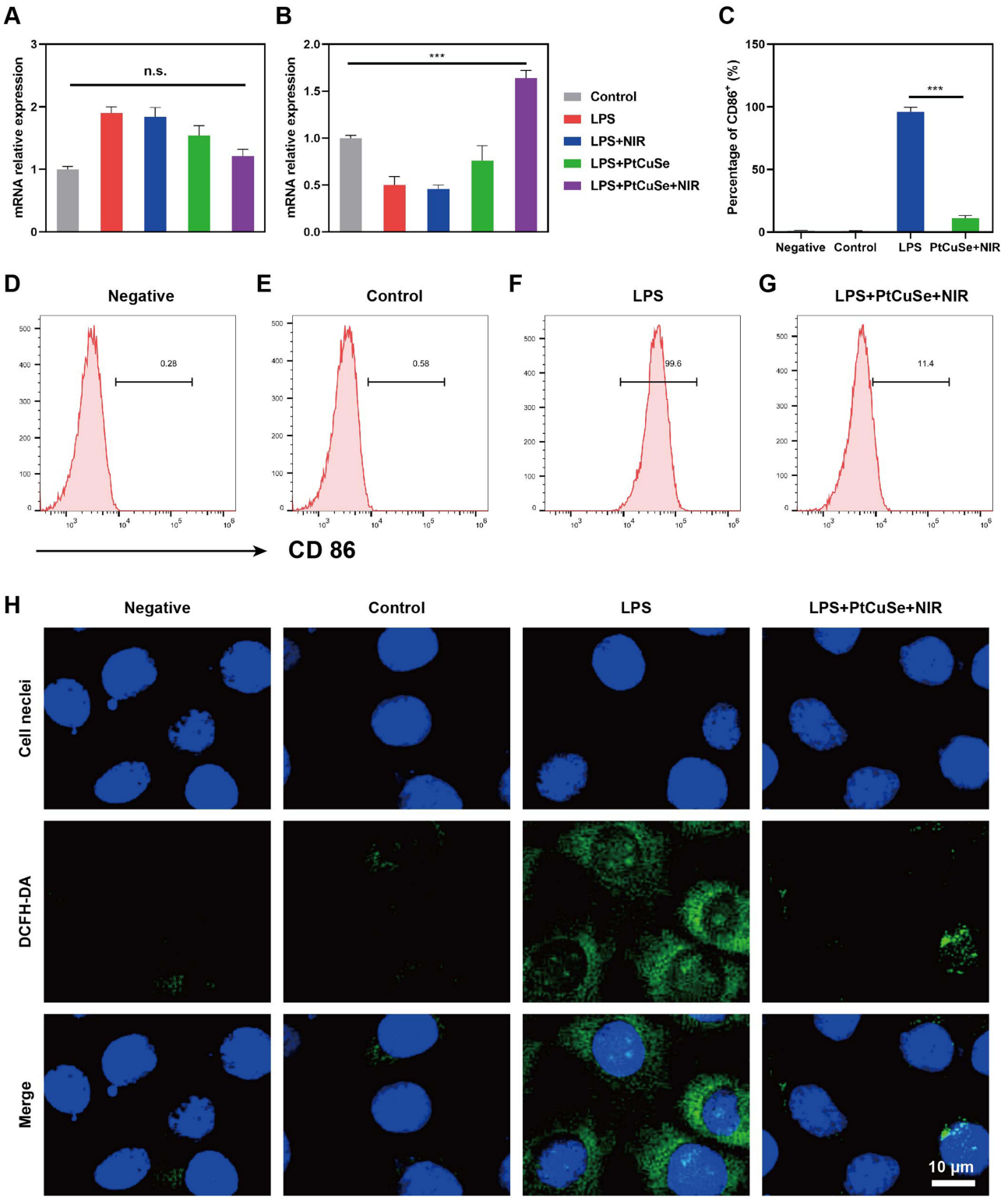

Figure 5 Evaluation of anti-inflammatory effects. qRT-PCR analysis of (**A**) TNF-α and (**B**) TGF-β in Raw 264.7 cell. (**C**) Percentage of CD86+ cells under various treatments. (**D**–**G**) Representative flow cytometry analysis pattern of CD86+ cells in various treatment groups. (**H**) Representative fluorescence images in various treatment groups using DCFH-DA probe. Data are presented as mean ± SD (n=3), *** p<0.001.

obvious green fluorescence was observed in LPS group. However, LPS+PtCuSe + NIR group showed significant reduction of ROS amount, indicating the anti-oxidant property of PtCuSe + NIR. These findings indicate that PtCuSe + NIR promotes the transformation of macrophages from the M1 type to the M2 type, thereby exerting anti-inflammatory effects.

Encouraged by the in vitro antibacterial and anti-inflammatory results of PtCuSe combined with NIR, the feasibility of this treatment for periodontitis was evaluated in vivo. First, PtCuSe hydrogel was applied on gingival sulcus of C57BL/6J and irradiated with laser. After 14 days, blood samples were obtained for further analysis. As shown in Figure S3, blood biochemical test data of control and PtCuSe + NIR group demonstrated no significant difference which suggest negligible systematic toxicity of PtCuSe + NIR. A periodontitis model was established in the right maxilla of C57BL/6J mice through surgical intervention. One week after model establishment, the mice were divided into five groups and subjected to various treatments. Following observation, the mice were sacrificed, and the maxillae, along with the teeth on the model side, were harvested for further analysis. Micro-computed tomography (micro-CT) was employed to assess the bone microstructure and morphology in detail (Figure 6A), while Hematoxylin and Eosin (H&E) staining was used to evaluate therapeutic effects (Figure 6B). Apparent alveolar bone loss was observed in both the PBS and NIR groups, with only slight improvement noted

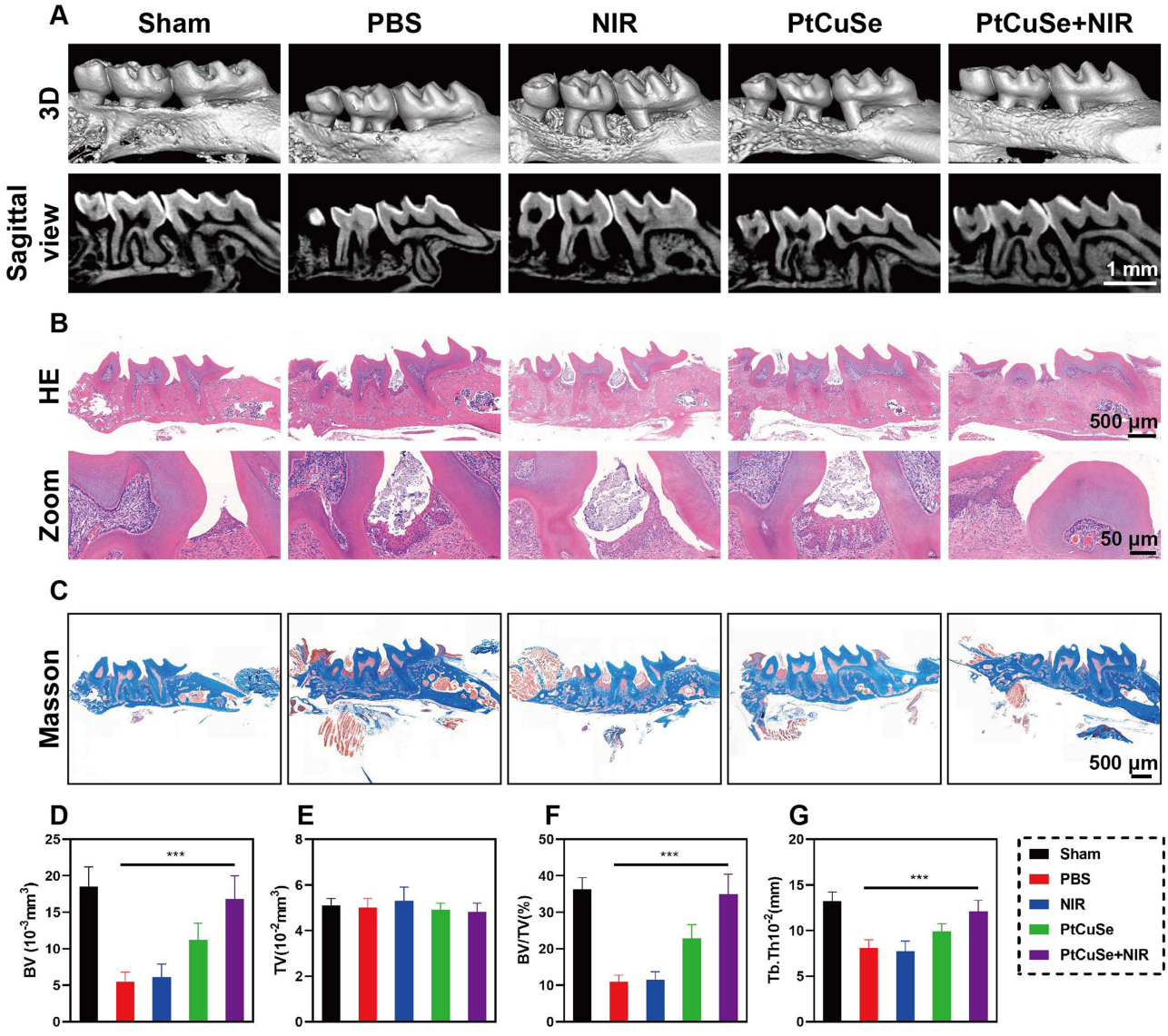

Figure 6 Evaluation of anti-periodontitis effects using mild photothermal therapy mediated by the PtCuSe nanozyme hydrogel. (**A**) 3D micro-CT reconstructed images and sagittal view of maxillary molars. (**B**) HE and (**C**) Masson staining images of periodontal tissue. (**D**)-(**G**) The quantitative statistics in various treatment groups. Data are presented as mean ± SD (n=3), F*** p<0.001.

https://doi.org/10.2147/IJN.S508864

in the PtCuSe group. In contrast, significant alleviation of bone resorption was observed in the PtCuSe + NIR group, attributed to the SOD-like activity of PtCuSe and the antibacterial effects of photothermal therapy. Compared to the sham group, both the PBS and NIR groups exhibited lymphocyte and granulocyte infiltration, along with a significant collagen loss. The PtCuSe group displayed connective tissue hyperplasia with minimal granulocyte infiltration. Masson staining confirmed higher positive area of 78% in PtCuSe + NIR group than other treatment groups (Figure 6C), confirming that periodontitis was alleviated. Quantitative analysis of bone properties and trabecular parameters in each treatment group is presented in Figure 6D–G. Bone volume (BV) significantly decreased in the PBS and NIR groups, indicating successful model establishment, while tissue volume (TV) showed no significant differences across all groups. Interestingly, BV and BV/TV returned to levels comparable to the sham group in the PtCuSe + NIR group. Trabecular thickness (Tb.Th), a key indicator of bone health and periodontitis progression, was quantified, showing that PtCuSe + NIR treatment significantly increased Tb.Th values. The results demonstrated that PtCuSe + NIR treatment could not only alleviate inflammation but also enhance bone recovery. In conclusion, photothermal therapy mediated by PtCuSe nanozyme hydrogel effectively enhances therapeutic efficacy against periodontitis through its antibacterial and anti-inflammatory activities.

Conclusion

In conclusion, a PtCuSe nanozyme hydrogel was fabricated for the treatment of periodontitis. Upon injection into the periodontal pocket, the nanozyme hydrogel underwent a sol-gel transformation, triggered by 808 nm laser irradiation, which was facilitated by the photothermal conversion properties of PtCuSe. The results of in vitro experiments demonstrated that, upon laser irradiation, PtCuSe displayed an improved antibacterial effect by effectively eliminating *P. gingivalis*, a key pathogen in periodontitis treatment. PtCuSe was found to scavenge significant amounts of ROS owing to its SOD- and CAT-like properties, which alleviated oxidative stress in the affected area. The treatment involving PtCuSe-mediated photothermal therapy was shown to polarize M1 macrophages into M2 macrophages, resulting in a reduction of pro-inflammatory cytokines, such as TNF-α, and an increase in anti-inflammatory cytokines, such as TGF-β, as verified by qT-PCR. In a mouse model of periodontitis, PtCuSe combined with NIR was found to prevent bone loss and enhance alveolar bone regeneration, attributed to the ROS-scavenging, antibacterial, and anti-inflammatory effects of the PtCuSe nanozyme hydrogel mediated by mild photothermal therapy. In addition, the PtCuSe hydrogel not only alleviates periodontitis but also reduces side effects by in situ release of nanozymes from a thermo-responsive hydrogel triggered by NIR. This study introduces an innovative approach to treating periodontitis through the use of a photothermal nanozyme hydrogel.

Acknowledgments

Please refer to the Supplementary File for detailed materials and methods.

Author Contributions

All authors made a significant contribution to the work reported, whether that is in the conception, study design, execution, acquisition of data, analysis and interpretation, or in all these areas; took part in drafting, revising or critically reviewing the article; gave final approval of the version to be published; have agreed on the journal to which the article has been submitted; and agree to be accountable for all aspects of the work.

Funding

This work was financially supported by the Basic Ability Enhancement Project for Young and Middle-aged Teachers in Guangxi Universities (2023KY0097), the Institution of National Natural Science Foundations of China (82160192) and Key Laboratory of Restoration and Reconstruction Research Guangxi open project (GXKLOMRR2410). Animal experiments in this work were performed according to the guidelines approved by the Medical Ethics Committee of Second Affiliated Hospital of Guangxi Medical University (Approval Number: 2024-KY (0813)).

Disclosure

The authors report no conflicts of interest in this work.

References

1. Nasiri K, Masoumi SM, Amini S, et al. Recent advances in metal nanoparticles to treat periodontitis. *J Nanobiotechnol*. 2023;21(1):283. doi:10.1186/s12951-023-02042-7
2. Kwon T, Lamster IB, Levin L. Current concepts in the management of periodontitis. *Int Dental J*. 2021;71(6):462–476. doi:10.1111/idj.12630
3. Trindade D, Carvalho R, Machado V, Chambrone L, Mendes JJ, Botelho J. Prevalence of periodontitis in dentate people between 2011 and 2020: a systematic review and meta-analysis of epidemiological studies. *J Clin Periodontol*. 2023;50(5):604–626. doi:10.1111/jcpe.13769
4. Sanz M, Marco Del Castillo A, Jepsen S, et al. Periodontitis and cardiovascular diseases: consensus report. *J Clin Periodontol*. 2020;47 (3):268–288. doi:10.1111/jcpe.13189
5. Rahimi A, Afshari Z. Periodontitis and cardiovascular disease: a literature review. *ARYA atherosclerosis*. 2021;17(5):1. doi:10.22122/arya.v17i0.2362
6. de Farias JO, de Freitas Lima SM, Rezende TMB. Physiopathology of nitric oxide in the oral environment and its biotechnological potential for new oral treatments: a literature review. *Clin Oral Investig*. 2020;24(12):4197–4212. doi:10.1007/s00784-020-03629-2
7. Di Stefano M, Polizzi A, Santonocito S, Romano A, Lombardi T, Isola G. Impact of oral microbiome in periodontal health and periodontitis: a critical review on prevention and treatment. *Int J mol Sci*. 2022;23(9):5142. doi:10.3390/ijms23095142
8. Sanz M, Herrera D, Kebschull M, et al. Treatment of stage I–III periodontitis—The EFP S3 level clinical practice guideline. *J Clin Periodontol*. 2020;47(S22):4–60. doi:10.1111/jcpe.13290
9. Cobb CM, Sottosanti JS. A re-evaluation of scaling and root planing. *J Periodontol*. 2021;92(10):1370–1378. doi:10.1002/JPER.20-0839
10. Hasuike A, Watanabe T, Hirooka A, et al. Enamel matrix derivative monotherapy versus combination therapy with bone grafts for periodontal intrabony defects: an updated review. *Japan Dent Sci Rev*. 2024;60:239–249. doi:10.1016/j.jdsr.2024.08.001
11. Lemberger M, Peterson P, Andlin Sobocki A, Setayesh H, Karsten A. Long-term radiographic and periodontal evaluations of the bone-grafted alveolar cleft region in young adults born with a UCLP. *Eur J Orthod*. 2024;46(1):cjad064. doi:10.1093/ejo/cjad064
12. Ng E, Tay JRH, Boey SK, Laine ML, Ivanovski S, Seneviratne CJ. Antibiotic resistance in the microbiota of periodontitis patients: an update of current findings. *Crit Rev Microbiol*. 2024;50(3):329–340. doi:10.1080/1040841X.2023.2197481
13. Ardila C-M, Bedoya-García J-A, Arrubla-Escobar D-E. Antibiotic resistance in periodontitis patients: a systematic scoping review of randomized clinical trials. *Oral Dis*. 2023;29(7):2501–2511. doi:10.1111/odi.14288
14. Ding Q, Wang Y, Wang T, et al. A natural polyphenolic nanoparticle--knotted hydrogel scavenger for osteoarthritis therapy. *Bioact Mater*. 2025;43:550–563. doi:10.1016/j.bioactmat.2024.09.037
15. Xiong Y, Li M, Qing G. Biomolecule-responsive polymers and their bio-applications. *Interdisciplinary Materials*. 2024;3(6):865–896. doi:10.1002/idm2.12210
16. Yang S, Zhu Y, Ji C, et al. A five-in-one novel MOF-modified injectable hydrogel with thermo-sensitive and adhesive properties for promoting alveolar bone repair in periodontitis: antibacterial, hemostasis, immune reprogramming, pro-osteo-/angiogenesis and recruitment. *Bioact Mater*. 2024;41:239–256. doi:10.1016/j.bioactmat.2024.07.016
17. El-Nablaway M, Rashed F, Taher ES, et al. Prospectives and challenges of nano-tailored biomaterials-assisted biological molecules delivery for tissue engineering purposes. *Life Sci*. 2024;349:122671. doi:10.1016/j.lfs.2024.122671
18. Nasser Atia GA, Barai HR, Shalaby HK, et al. Baghdadite: a novel and promising calcium silicate in regenerative dentistry and medicine. *ACS Omega*. 2022;7(49):44532–44541. doi:10.1021/acsomega.2c05596
19. Atia GA, Shalaby HK, Roomi AB, et al. Macro, micro, and nano-inspired bioactive polymeric biomaterials in therapeutic, and regenerative orofacial applications. *Drug Des Devel Ther*. 2023;17:2985–3021. doi:10.2147/DDDT.S419361
20. Atia GA, Shalaby HK, Ali NG, et al. New challenges and prospective applications of three-dimensional bioactive polymeric hydrogels in oral and craniofacial tissue engineering: a narrative review. *Pharmaceuticals*. 2023;16(5):702. doi:10.3390/ph16050702
21. El-Nablaway M, Rashed F, Taher ES, et al. Prospective and challenges of locally applied repurposed pharmaceuticals for periodontal tissue regeneration. *Front bioeng biotechnol*. 2024;12:1400472
22. Atia GA, Rashed F, Taher ES, et al. Challenges of therapeutic applications and regenerative capacities of urine based stem cells in oral, and maxillofacial reconstruction. *Biomed Pharmacother*. 2024;177:117005. doi:10.1016/j.biopha.2024.117005
23. El-Nablaway M, Rashed F, Taher ES, et al. Bioactive injectable mucoadhesive thermosensitive natural polymeric hydrogels for oral bone and periodontal regeneration. *Front bioeng biotechnol*. 2024;12: 1384326.
24. Johnson A, Kong F, Miao S, Thomas S, Ansar S, Kong Z-L. In-vitro antibacterial and anti-inflammatory effects of surfactin-loaded nanoparticles for periodontitis treatment. *Nanomaterials*. 2021;11(2):356. doi:10.3390/nano11020356
25. Zhou J, Fang C, Rong C, Luo T, Liu J, Zhang K. Reactive oxygen species-sensitive materials: a promising strategy for regulating inflammation and favoring tissue regeneration. *Smart Mater Med*. 2023;4:427–446. doi:10.1016/j.smaim.2023.01.004
26. Wang H, Wang D, Huangfu H, et al. Branched AuAg nanoparticles coated by metal–phenolic networks for treating bacteria-induced periodontitis via photothermal antibacterial and immunotherapy. *Mater Des*. 2022;224:111401. doi:10.1016/j.matdes.2022.111401
27. Wang P, Wang L, Zhan Y, et al. Versatile hybrid nanoplatforms for treating periodontitis with chemical/photothermal therapy and reactive oxygen species scavenging. *Chem Eng J*. 2023;463:142293. doi:10.1016/j.cej.2023.142293
28. Zhang C, Yan R, Bai M, et al. Pt-clusters-equipped antioxidase-like biocatalysts as efficient ros scavengers for treating periodontitis. *Small*. 2024;20 (17):2306966. doi:10.1002/smll.202306966
29. Ren S, Zhou Y, Fan R, et al. Constructing biocompatible MSN@Ce@PEG nanoplatform for enhancing regenerative capability of stem cell via ROS-scavenging in periodontitis. *Chem Eng J*. 2021;423:130207. doi:10.1016/j.cej.2021.130207
30. Tian M, Chen G, Xu J, et al. Epigallocatechin gallate-based nanoparticles with reactive oxygen species scavenging property for effective chronic periodontitis treatment. *Chem Eng J*. 2022;433:132197. doi:10.1016/j.cej.2021.132197
31. Ren S, Zhou Y, Zheng K, et al. Cerium oxide nanoparticles loaded nanofibrous membranes promote bone regeneration for periodontal tissue engineering. *Bioact Mater*. 2022;7:242–253. doi:10.1016/j.bioactmat.2021.05.037
32. Xu Y, Luo Y, Weng Z, et al. Microenvironment-responsive metal-phenolic nanozyme release platform with antibacterial, ROS Scavenging, and osteogenesis for periodontitis. *ACS Nano*. 2023;17(19):18732–18746. doi:10.1021/acsnano.3c01940

33. Zhu B, Wu J, Li T, et al. A glutathione peroxidase-mimicking nanozyme precisely alleviates reactive oxygen species and promotes periodontal bone regeneration. *Adv Healthcare Mater*. 2024;13(4):2302485. doi:10.1002/adhm.202302485
34. Sun J, Wang J, Hu W, et al. A porous bimetallic Au@pt core–shell oxygen generator to enhance hypoxia-dampened tumor chemotherapy synergized with NIR-II photothermal therapy. *ACS Nano*. 2022;16(7):10711–10728. doi:10.1021/acsnano.2c02528
35. Han HH, Kim S-J, Kim J, et al. Bimetallic hyaluronate-modified Au@Pt nanoparticles for noninvasive photoacoustic imaging and photothermal therapy of skin cancer. *ACS Appl Mater Interfaces*. 2023;15(9):11609–11620. doi:10.1021/acsami.3c01858
36. Lyu M, Zhu D, Duo Y, Li Y, Quan H. Bimetallic nanodots for tri-modal CT/MRI/PA imaging and hypoxia-resistant thermoradiotherapy in the NIR-II biological windows. *Biomaterials*. 2020;233:119656. doi:10.1016/j.biomaterials.2019.119656
37. Yu J, Yang L, Yan J, et al. Carbon nanomaterials for photothermal therapies. *Carbon Nanomaterials Bioimaging Bioanalysis Ther*. 2019:309–340.
38. Huang Z, Cui X, Li S, et al. Two-dimensional MXene-based materials for photothermal therapy. *Nanophotonics*. 2020;9(8):2233–2249.
39. Xie Z, Peng M, Lu R, et al. Black phosphorus-based photothermal therapy with aCD47-mediated immune checkpoint blockade for enhanced cancer immunotherapy. *Light Sci Appl*. 2020;9(1):161. doi:10.1038/s41377-020-00388-3
40. Qing G, Zhao X, Gong N, et al. Thermo-responsive triple-function nanotransporter for efficient chemo-photothermal therapy of multidrug-resistant bacterial infection. *Nat Commun*. 2019;10(1):4336. doi:10.1038/s41467-019-12313-3
41. Chen W, Wang Y, Qin M, et al. Bacteria-driven hypoxia targeting for combined biotherapy and photothermal therapy. *ACS Nano*. 2018;12 (6):5995–6005. doi:10.1021/acsnano.8b02235
42. Kim H, Lee YR, Jeong H, et al. Photodynamic and photothermal therapies for bacterial infection treatment. *Smart Molecules*. 2023;1(1): e20220010. doi:10.1002/smo.20220010
43. Wang S-B, Liu X-H, Li B, et al. Bacteria-assisted selective photothermal therapy for precise tumor inhibition. *Adv Funct Mater*. 2019;29 (35):1904093. doi:10.1002/adfm.201904093
44. Huo J, Jia Q, Huang H, et al. Emerging photothermal-derived multimodal synergistic therapy in combating bacterial infections. *Chem Soc Rev*. 2021;50(15):8762–8789. doi:10.1039/D1CS00074H
45. Zhang Y, Gao W, Ma Y, et al. Integrating Pt nanoparticles with carbon nanodots to achieve robust cascade superoxide dismutase-catalase nanozyme for antioxidant therapy. *Nano Today*. 2023;49:101768. doi:10.1016/j.nantod.2023.101768
46. Zhang X-L, Gu -Y-Y, Liu Y-C, et al. Near-infrared enhanced organic Se-doped carbon nitride quantum dots nanozymes as SOD/CAT mimics for anti-Parkinson via ROS-NF-κB-NLRP3 inflammasome axis. *Chem Eng J*. 2024;499:156028. doi:10.1016/j.cej.2024.156028
47. Lin S, Cheng Y, Zhang H, et al. Copper tannic acid coordination nanosheet: a potent nanozyme for scavenging ros from cigarette smoke. *Small*. 2020;16(27):1902123. doi:10.1002/smll.201902123